Polymer Degradation and Stability 243 (2026) 111778

Contents lists available at ScienceDirect

Polymer Degradation and Stability

journal homepage: www.journals.elsevier.com/polymer-degradation-and-stability

Biodegradable and biocompatible polyesters based on poly(butylene succinate) and poly(hexamethylene diglycolate) with shape memory features for potential use in corneal surgery

Arianna Palumbo [a], Gloria Astolfi [b], Michelina Soccio [a], Giulia Guidotti [a,*], Elisa Boanini [c], Elisabetta Salatelli [d], Piera Versura [b], Nadia Lotti [a]

[a] Department of Civil, Chemical, Environmental and Materials Engineering (DICAM), University of Bologna, Italy
[b] Ophthalmology Unit, DIMEC, Alma Mater Studiorum Università di Bologna, Italy
[c] Department of Chemistry "Giacomo Ciamician", University of Bologna, Via Gobetti 85, 40129 Bologna, Italy
[d] Department of Industrial Chemistry "Toso Montanari", University of Bologna, Viale Risorgimento 4, 40136 Bologna, Italy

ARTICLE INFO

Keywords:
Polyesters
Poly(butylene succinate)
Poly(hexamethylene diglycolate)
Shape memory
Corneal surgery
Biocompatibility
Biodegradation

ABSTRACT

Nowadays, interventions in ophthalmic surgery, in particular corneal ones, are countless. Regardless of the type, the success of each intervention is largely due to the correct positioning and tightness of the suture. The achievement of these goals is particularly challenging, although extensive research has been carried out to design new materials with suitable features, including shape memory ones. Among all synthetic polymers, aliphatic polyesters are credible solutions for the realization of biocompatible sutures, as they are easy to process and show a very high degree of customization. Accordingly, in the present study, poly(butylene succinate) (PBS), a biocompatible and biodegradable aliphatic polyester, was chosen as the reference homopolymer. In order to lower its high rigidity and improve the low degradation rate, it was physically and chemically mixed with poly (hexamethylene diglycolate) (PHDG), another aliphatic polyester containing ether oxygens in its main chain. The new materials obtained showed intermediate properties, especially from a thermal and mechanical point of view, depending on the molecular architecture. The introduction of PHDG, in addition to not interfering with the biocompatibility of PBS, also allowed for an increase in its degradation rate. Last, but not least, the obtained materials showed qualitative shape memory features.

1. Introduction

The eye is a highly sensitive organ that enables vision by capturing light and converting it into electrical signals, which are then transferred to the brain [1]. This organ is as important as delicate, being affected by many different diseases [2]. According to World Health Organization [3], >2.2 billion people worldwide experience some form of visual impairment, and nearly half of these cases could be prevented from progressing to blindness. Ocular diseases, in particular those related to cornea, such as corneal opacity [4], also have a significant impact on patients' quality of life, often leading to severe limitations in daily activities [5,6] and lifelong impact [7]. This is not only a social problem: it has been estimated that the approximately 45 million people suffering from blindness related to corneal diseases, impose an economic burden of about $600 billion [8,9]. Nowadays, big steps have been taken in the field of ophthalmic surgery, and the interventions focused on limiting visual impairment and restoring corneal functionality are countless, most of them requiring proper suturing [10]. Effective suturing is essential for successful outcomes in corneal surgery, especially anterior lamellar keratoplasty and full-thickness transplantation [10]. The two main suture materials currently used for corneal transplantation are nylon and Mersilene [11]. Nylon sutures are easy to control, with minimal complications in the first two years after surgery [12]. Mersilene, a polyester monofilament, is neither hydrolysed nor degraded by ultraviolet light, and is classified as non-biodegradable. Although it leads to fewer cases of postoperative astigmatism compared to nylon, it is more difficult to handle and requires adjustments in suture tension [12,13]. Moreover, with the aim of minimising postoperative complications and

* Corresponding author.
E-mail addresses: arianna.palumbo3@unibo.it (A. Palumbo), gloria.astolfi2@unibo.it (G. Astolfi), m.soccio@unibo.it (M. Soccio), giulia.guidotti9@unibo.it (G. Guidotti), elisa.boanini@unibo.it (E. Boanini), elisabetta.salatelli@unibo.it (E. Salatelli), piera.versura@unibo.it (P. Versura), nadia.lotti@unibo.it (N. Lotti).

https://doi.org/10.1016/j.polymdegradstab.2025.111778
Received 12 September 2025; Received in revised form 23 October 2025; Accepted 10 November 2025
Available online 11 November 2025

avoiding the need for subsequent suture removal procedures, a good alterative solution could be the use of either a combination of non-resorbable and resorbable sutures [10,14] or fully resorbable ones [15–19].

Absorbable sutures, which are becoming increasingly popular in ophthalmic surgery, are devices designed to degrade completely within approximately 3 to 6 months from implantation, at the same rate at which tissue strength gradually recovers [20,21]. Synthetic absorbable sutures mainly undergo hydrolytic degradation, where polymer chains break down into low-molecular-weight products easily metabolised or eliminated by human body [22]. Several factors influence the rate of this process, including the polymer's structure, degree of crystallinity, pH level at the implantation site, temperature, tissue type and local salt composition [23].

Polyesters are one of the most suitable class of polymers for producing resorbable sutures. Several resorbable sutures are already commercially available; the most notable are Vicryl, which is made from a glycolide-lactide copolymer, and Dexon, which is made from polyglycolic acid [24,25]. However, they lack of the capability of properly adjust their shape *in-situ*, in order to provide the proper suture tension once placed. This feature can be achieved with the use of shape-memory materials.

Shape memory is defined as the ability of a material to recover its original shape from a temporary one, which is generally characterised by significant deformation, when a particular stimulus is applied [26,27]. For applications inside the human body, as in the case of sutures, a useful stimulus may be body temperature. The shape-memory effect is not an intrinsic property of polymers, but rather requires specific processing steps [28]. Indeed, to fix the permanent form of a material, cross-linking is required. This can be chemical, which makes the material thermosetting and insoluble, or physical, this last resulting from the presence of crystalline phases which melt at a proper temperature. However, these alone are not sufficient to ensure shape memory behaviour. In addition to the hard crystalline regions that fix the permanent shape, soft regions are also required, to allow the transition to the temporary shape [29,30].

According to this complex scenario, the present work focuses on the *ad-hoc* design of new aliphatic polyesters, which can be potential candidates as shape memory materials, to be used in ophthalmic surgery. More in detail, poly(butylene succinate) (PBS) has been selected as the material that can maintain the permanent shape. This polyester has been widely studied in previous literature, including by the research group that authored this work [31–34]. It has also been investigated for potential applications in the biomedical field, as drug delivery material or for tissue engineering [35–37]. PBS is characterised by high crystallinity and mechanical rigidity, and its melting temperature is among the highest inside the family of aliphatic polyesters. However, it degrades slowly and cannot be used on its own to obtain resorbable and shape-memory sutures [31]. For this reason, PBS has been physically and chemically modified with poly(hexamethylene diglycolate) (PHDG). PHDG, which contains ether oxygen atoms in its macromolecular chain has a lower melting point than PBS, close to body temperature, and is also more flexible [38]; these characteristics make it suitable for use as a soft phase in shape memory materials. Furthermore, ether oxygen atoms increase polyester hydrophilicity [39] and promote its degradation [40].

Therefore, an equiponderal physical blend and copolymers with different block lengths were prepared and processed in thin films. The molecular, structural, thermal and mechanical properties were analysed to determine property-structure correlations. Surface wettability, hydrolytic degradation, qualitative shape memory analysis and preliminary biocompatibility tests using corneal cell line were also carried out, to verify their potential suitability as value-added materials in the ophthalmic field.

2. Materials and methods

2.1. Materials

Dimethyl succinate (DMS), diglycolic acid (DGA), 1,4-butanediol (BD) and titanium tetrabutoxide (TBT) were purchased from Sigma-Aldrich (Saint Louis, MO, USA); 1,6-hexanediol (HD) was purchased from TCI (Zwijndrecht, Belgium). All the reagents were reagent-grade.

2.2. Poly(butylene succinate) and poly(hexamethylene diglycolate) synthesis

The synthesis of poly(butylene succinate) (PBS), and poly(hexamethylene diglycolate) (PHDG) was carried out by two-step melt polycondensation in a glass reactor, continuously stirred (100 rpm), and put in a thermostated silicon oil bath. The starting monomers were DMS and BD, and DGA and HD, respectively (glycolic molar excess of about 20 %), together with 200 ppm of TBT, used as catalyst. In brief, during the first step, esterification or transesterification reactions (depending on whether the starting monomers were the diacid or the diester, respectively) occurred under a pure nitrogen flow at a temperature of 180 °C, while water or methanol, respectively, was distilled off (1.5 h). The second step was carried out under high vacuum (0.048 mbar) at a temperature of 200 °C, in order to eliminate the glycolic excess, favouring the increase in molecular weight. A gradual increase in torque was observed during this phase, which lasted for about 3 additional hours. The synthesis was stopped when torque reached a plateau value, and the high molecular weight polymer was obtained.

2.3. Blend and copolymers preparation and processing

After synthesis, a binary mixture was prepared starting from 50/50 wt amounts of the two homopolymers. The polymers were dissolved, under magnetic stirring at room temperature, in the minimum amount of chloroform. The resulting solution was then poured into Petri dishes to allow solvent evaporation.

Poly(butylene succinate-co-hexamethylene diglycolate) copolymers were obtained by reactive blending starting from the previously prepared equiponderal blend at 225 °C and using as catalyst the residual TBT inside the homopolymers. A controlled nitrogen flow and constant stirring at 50 rpm were applied. Exploratory reactive blending was performed to observe changes in the molecular architecture of the copolymers at different mixing times, 5 min, 20 min and 2 h, respectively.

Samples were designated as PBS/PHDG for the blend, and P(BS-HDG)x for the copolymers, where x represents the mixing time.

Before being tested, all the samples were processed into films (about 100 μm thick) by compression moulding, using a Carver (Wabash, IN, USA) C12 laboratory press. About 1.7 g of each material was put in between two Teflon sheets inside the press and heated to a temperature 20 °C higher than the melting temperature. After 2 min a pressure of 2.5 ton/m^2 was applied and maintained for 2 min. Then, the films were ballistically cooled, in press, to room temperature.

2.4. Molecular characterisation

The chemical structure of copolymers was confirmed by proton nuclear magnetic resonance spectroscopy (^{1}H NMR) using an Agilent Varian Inova 400 MHz instrument (Palo Alto, CA, USA). Measurements were carried out at room temperature. Samples were prepared by dissolving about 10 mg of material in 0.7 mL of deuterated chloroform containing 0.03 vol % tetramethylsilane (TMS) as internal standard. For ^{13}C NMR experiments, conducted to determine the length of copolymer sequences, 30 mg of material was used instead of 10 mg.

The molecular weights (M_n) and the corresponding polydispersity indexes (D) were evaluated at 25 °C by gel permeation chromatography (GPC) using an HPLC Lab Flow 2000 apparatus (Waters, Milford, MA,

USA) equipped with a Rheodyne 7725i injector (Thermo Fisher Scientific, Waltham, MA, USA), a Phenomenex (Torrence, CA, USA) Phenogel MXM 5 μm mixed-bed column, and an RI K-2301 (KNAUER, Berlin, Germany) detector. The instrument was calibrated with polystyrene standards in the range of 550–2500,000 g/mol. HPLC-grade chloroform was used as the eluent, with a flow of 1 mL/min. The samples were prepared by dissolution in the same solvent used as the eluent (2 mg/mL).

2.5. Morphological characterisation

To evaluate the compatibility of the two homopolymers inside the blend and the copolymer with longer blocks, the morphological characterisation of cryo-fractured cross-sections of each sample was performed using a Zeiss Leo-1530 scanning electron microscope (SEM), operating at 5 kV. The analyses were carried out after the deposition of a gold conductive coating.

2.6. Thermal and structural characterisation

TGA measurements were performed by means of a Perkin Elmer (Waltham, MA, USA) TGA4000, equipped with Pyris 11 software, under a pure N_2 flow (40 mL/min). About 8 mg of material was heated at a constant rate of 10 °C/min in the temperature range of 40–800 °C. T_{onset} was calculated as the temperature corresponding to the beginning of degradation, while T_{max} was calculated as the minimum of the thermogram derivative.

Differential scanning calorimetry was performed using a Perkin Elmer (Waltham, MA, USA) DSC6 under pure N_2 flow (20 mL/min). About 5 mg of each sample was placed in aluminium pans and subjected to the following thermal programme controlled by Pyris 11 software: heating from −70 to 180 °C at 20 °C/min (I scan), rapid cooling from 180 to −70 °C at 100 °C/min, and subsequent heating from −70 to 180 °C at 20 °C/min (II scan). The glass transition temperature (T_g) was calculated as the midpoint of the glass-to-rubber transition step, while the relative specific heat increment (ΔC_p) was determined as the height between the two baselines related to the glass-to-rubber transition step. The melting temperature (T_m) and the cold crystallization temperature (T_{cc}) were calculated as the maximum/minimum of the endotherms/exotherms in the DSC traces, respectively, while the corresponding heat of melting (ΔH_m) and heat of crystallization (ΔH_{cc}) were obtained from the areas of the endothermic and exothermic phenomena, respectively. In order to determine the crystallization capability under non-isothermal conditions, the samples were heated at 20 °C/min to about 40 °C above melting temperature, kept there for 3 min and then cooled at 10 °C/min.

Wide-angle X-ray scattering (WAXS) experiments were carried out on all the films using a PANalytical (Almelo, The Netherlands) X'PertPro diffractometer coupled with a copper source (λ = 0.154 nm) and equipped with a solid-state X'Celerator detector (0.1° steps, rate = 100 s/step). The crystallinity degree (X_c) was calculated as the ratio between the crystalline diffraction area (A_c), obtained by subtracting the amorphous halo from the total area of the diffraction profile, and the area of the whole diffraction profile (A_t).

2.7. Mechanical characterisation

Tensile tests were performed using an Instron (Norwood, MA, USA) 5966 dynamometer, equipped with rubber grips and a transducer-coupled 1 kN load cell. Measurements were performed on rectangular film specimens (5 mm × 50 mm, gauge length of 20 mm), which were stretched at a rate of 10 mm/min. The instrument measures the load applied as a function of the displacement (which is calculated as the ratio between the length variation and the initial one) and can convert these data into stress–strain curves. The elastic modulus (E) was calculated as the slope of the initial linear segment of the curve without the use of any extensometer, while the stress at break (σ_B) and elongation at break (ε_B) were determined as the values of stress and elongation at the breakpoint. At least 5 specimens were tested for each material, and the results obtained are reported as the average value ± standard deviation. Cyclic tests were also performed to evaluate the elastic return: samples without yielding points were strained and released (21 cycles at 10 mm/min) to get 8–18 % elongation.

2.8. Qualitative memory shape evaluation

To qualitatively verify that the blend and the copolymer with longer blocks have shape memory properties, a temporary shape was induced on rectangular strips of each film. More in detail, the strips were placed in an oven at a temperature of 60 °C for 15 min. As soon as they were removed from the oven, a temporary shape, in this case a spiral shape, was induced. Finally, the strips in their temporary shape were stored at a temperature of 4 °C for at least 4 days to allow the PHDG to recrystallize. To verify the shape memory behaviour, they were immersed in water at a temperature of 60 °C, corresponding to the temperature used to induce the temporary shape.

2.9. Surface wettability measurements

Static water contact angle (WCA) measurements were carried out at room temperature on polymeric films by means of a Krüss DSA30S instrument. The side profiles of the deionized water drop (4 μL) were recorded and analysed immediately after drop deposition using Drop Shape Analysis software. The deposition of at least eight different drops was performed on different surface areas, and WCA values were reported as the average value ± standard deviation.

2.10. Hydrolytic degradation tests

Hydrolytic degradation experiments were performed by incubating polymeric films (5 × 25 mm) in phosphate buffered saline solution (pH = 7.4) and 37 °C in a shaking incubator (Stuart SI500). The buffer solution was periodically changed to keep the pH constant. At different time intervals (every 30 days, for 6 months), duplicate specimens for each sample were recovered from the incubator, repeatedly washed with deionised water, and dried for 2 days to reach constant weight. Weight loss was determined by comparing the residual dry weight at a specific time with the initial weight. Molecular weight loss data were obtained by gel-permeation chromatography (GPC) at 30 °C and thermal properties of partially degraded samples were studied using differential scanning calorimetry (DSC), as in previous analyses.

2.11. Biocompatibility tests

Samples preparation: The PBS/PHDG blend and the P(BS-HDG)5 block copolymer were purified through dissolution in chloroform and precipitation dropwise in methanol, in order to remove the residual catalyst and possible byproducts. The materials were then processed into films, as before. These polymeric films (surface of approximately 0.5 cm^2) were sterilized through immersion in a solution of 90 % v/v ethanol for 30 min, followed by immersion in a 70 % v/v ethanol solution for further 30 min. Subsequently, each piece of film was washed in phosphate buffered saline, pH 7.4.

Cell culture: Primary human corneal fibroblasts (phCornF) derived from normal human corneal tissue were seeded in 24-well culture plates (with or without films) at a density of 2×10^4 cells per well and in 96 well culture plates at a density of 5×10^2 in Dulbecco's modified Eagle's medium (DMEM, Gibco) supplemented with 10 % fetal bovine serum (Gibco, ThermoFisher Scientific 168 Third Avenue Waltham, MA USA), 1 mM L-glutamine, penicillin (20,000 U/ml) and streptomycin (20,000 mg/ ml, Lonza Group Ltd, Basel, Switzerland), under a CO_2 (5 %) atmosphere at 37 °C. Cells from passages 1 through 5 were used. The

normal culture development, the morphology and the level of confluence were assessed daily by observation under an inverted light microscope (ZEISS Axiocam 208 color camera).

Cytocompatibility tests: Cytotoxicity tests were performed according to the experimental procedures described in ISO 10,993–5 [41]. At the end of three different incubation times (24, 48, and 72 h), the number of live cells could be quantified by the 3-(4,5-dimethyl-2-thiazolyl)-2, 5-diphenyl-tetrazoluim bromide (MTT) assay. Briefly, each sample was incubated for two hours at 37 °C in the presence of 0.5 mg/mL MTT solution in DMEM, and then 100 mL of isopropanol was added to each well to dissolve the formazan dye. The solutions were transferred to a 96-well plate, and the absorbance was measured at 570 nm using a Multiskan SkyHigh microplate reader (ThermoFisher Scientific).

Direct contact method: Small polymeric films (0.5 cm^2/well) were placed in the centre of subconfluent phCornF monolayers in 24-well plates, which covered one-tenth of the surface area, according to established standards [41]. The same procedure was followed using NaCl 1500 mOsm as a positive control, while cells not exposed to any biomaterials served as a negative control. The cell–material contact was maintained for 24, 48 and 72 h at 37 °C and 5 % CO_2.

Test on extracts: Control samples (commercial poly(butylene succinate) (Mitzubishi chemical corporation) C-PBS), synthetised PBS (PBS), the physical blend (PBS/PHDG) and the block copolymer (P(BS-HDG)5) were prepared by incubating the films in DMEM containing 5 % fetal bovine serum and 1 % penicillin-streptomycin for 24 h (37 °C, 5 % CO_2). Next day, 100 μL of control and polymer extracts were added to each well of a 96-well culture plate after removal of equal amounts of medium and incubated at the same conditions of direct contact tests.

Statistics and analysis: Data are expressed as means ± standard deviations of a representative of three experiments carried out in triplicate. The analysis was performed using One-way ANOVA tests by the GraphPad Prism 10.0 software (CA, USA) and $p < 0.05$ was considered as statistically significant.

3. Results and discussion

3.1. Synthesis and molecular characterisation

Fig. 1 illustrates the Scheme of the workflow leading to the production of the blend and block copolymer-based films together with some the functional properties of the obtained films. At room temperature, poly(butylene succinate) (PBS) and poly(hexamethylene diglycolate) (PHDG) appear as light yellow, semicrystalline solids. The equiponderal physical blend is quite transparent, flexible and light in colour. The copolymers obtained by reactive blending at different times, i.e. 5, 20 and 120 min, appear progressively more flexible and of an increasingly intense yellow colour. Moreover, all the materials were easily soluble in chloroform, allowing the exclude the occurrence of any crosslinking during the synthetic procedure.

The chemical structure of the homopolymer, the physical blend and all the copolymers was confirmed by ^{1}H NMR spectroscopy. In Fig. S1 P (BS-HDG)5 spectrum is shown as an example. As in all the other ^{1}H NMR spectra, in addition to the signal of chloroform at δ 7.26 ppm and TMS at δ 0 ppm, the singlet of methylene protons related to succinic acid *a* at δ 2.61 ppm and the singlet of methylene protons related to diglycolic acid *d* at δ 4.23 ppm can be detected. In addition, the signals of the methylene protons of butanediol subunit *b* (triplet) and *c* (multiplet) are located at δ 4.09 ppm and δ 1.68 ppm, respectively. As to the hydrogen atoms of hexanediol subunit, *e, f* and *g*, they are recorded at δ 4.13 ppm (triplet), δ 1.64 ppm (multiplet), and δ 1.35 ppm (multiplet), respectively.

Since the copolymers obtained by reactive mixing have the same weight composition but different block lengths, ^{13}C NMR spectroscopy was carried out to better highlight the so-called mixed forms, signals that appear in the NMR spectrum when the transesterification reactions take place and the block lengths get progressively shorter. As an example, in Fig. 2 the ^{13}C NMR spectrum of P(BS-HDG)5 with the corresponding peaks' assignment is reported, while in Fig. S2 all the ^{13}C NMR spectra are shown. The spectra obtained were consistent with the predicted structure, as only the peaks related to the carbons within each

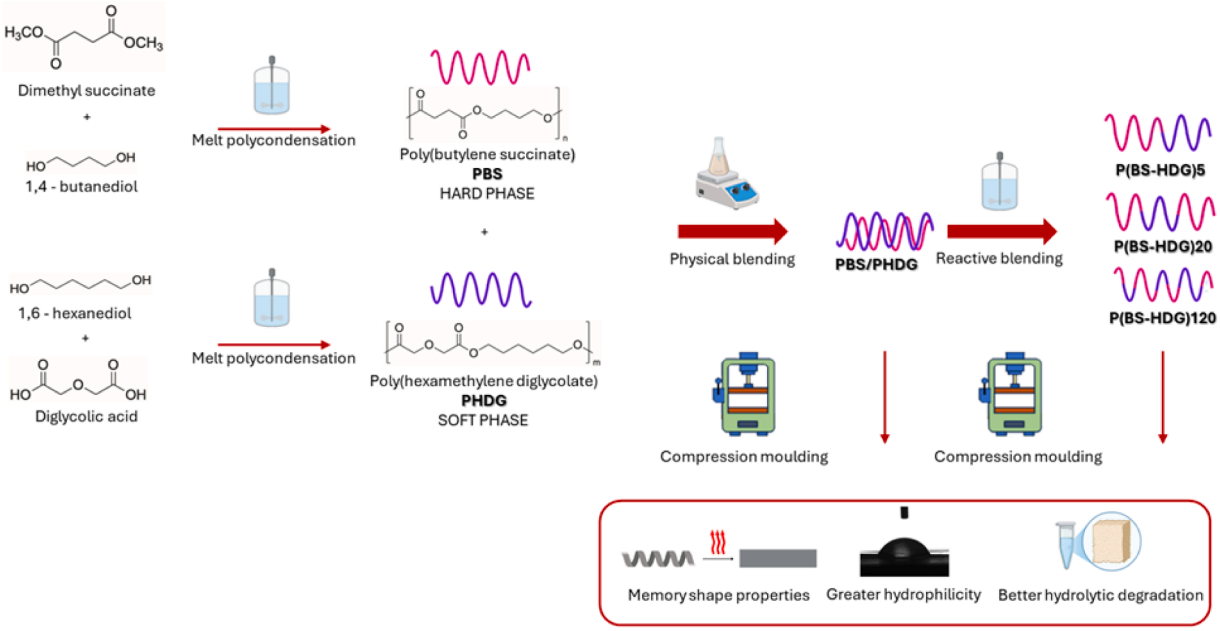

Fig. 1. A schematic representation of the overall work. On the left the monomers used to synthesise the PBS and PHDG homopolymers, followed by the preparation of the physical mixture and the synthesis of the P(BS-HDG)x copolymers. At the bottom the effects of adding PHDG to the polymer system on the most important properties.

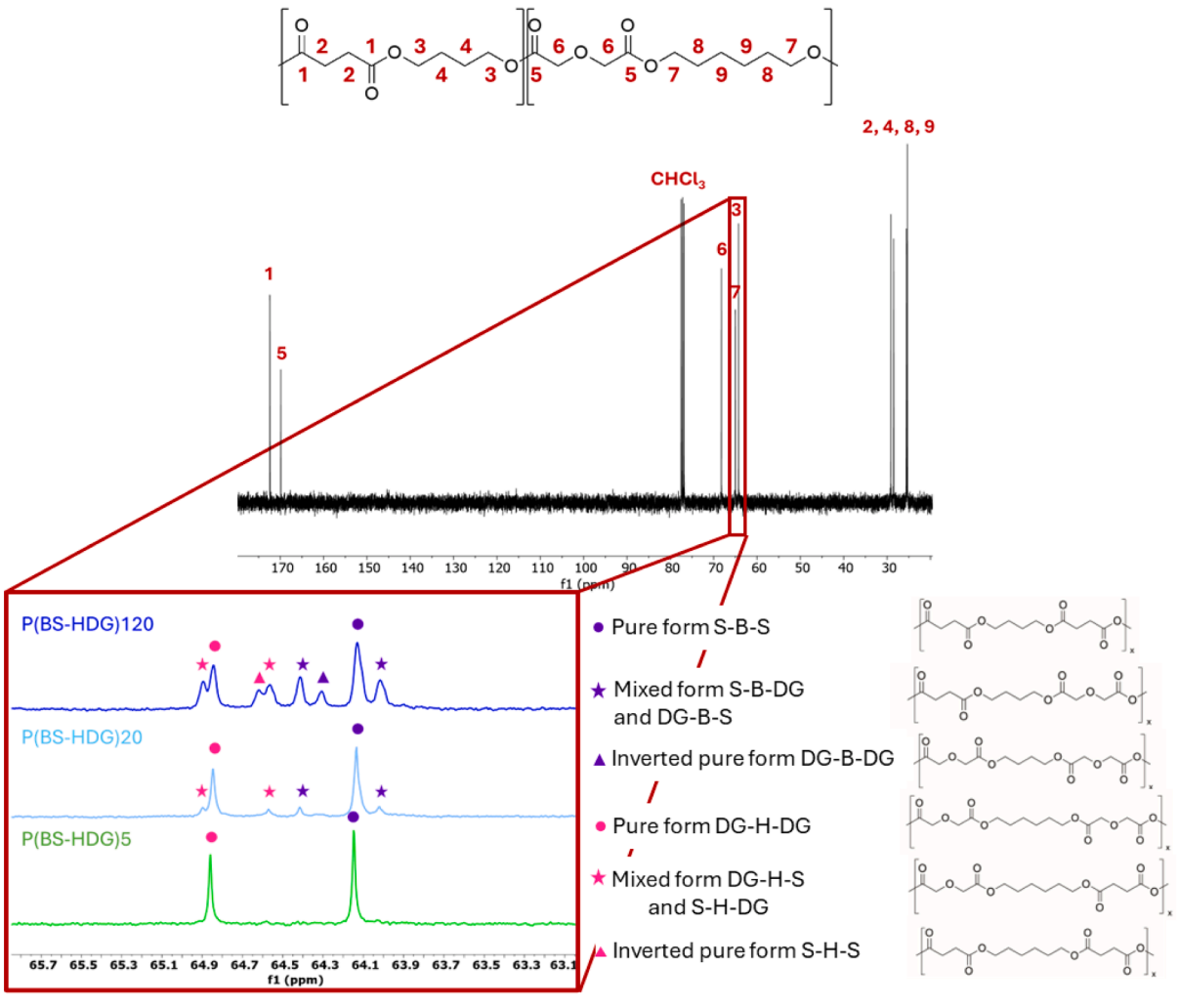

Fig. 2. ^{13}C NMR spectrum of P(BS-HDG)5 copolymer with peaks' assignment and zooming of the zone 63.2–65.7 ppm to highlight the occurrence of mixed forms, the chemical structures of which are also shown.

chemical structure were visible, allowing to exclude the occurrence of any secondary reactions during the synthesis, such as branching. More in detail, in addition to the peaks related to chloroform at δ 77 ppm, peak *1* at δ 172 ppm corresponding to the carbonyl carbons of PBS and peak *5* at δ 169 corresponding to the carbonyl carbons of PHDG can be detected. The signal relating the carbon atoms in α to the ester oxygen of PBS (3) is located at δ 64.1 ppm, while that of PHDG (*7*) at δ 64.9 ppm. At δ 69 ppm signal *6*, which is due to the carbon atoms in α to the carbonyl of diglycolic acid, appears. The signals of the other carbon atoms *2, 4, 8* and *9*, related to the carbon atoms in α to the carbonyl of succinic acid and to the inner carbons of the glycolic subunits of butanediol and hexanediol, respectively, fall in the range between δ 29 ppm and δ 26 ppm

In Fig. 2a zooming of the region between δ = 63.2 ppm and δ = 65.7 ppm of the ^{13}C NMR spectra of three different copolymers is also reported. In this region, the signals corresponding to the carbon atoms in α to the ester oxygen of the copolymers can be seen. As the reactive blending proceeds, many different signals become evident: apart from the peak corresponding to S-B-S sequences (pure form, δ 64.15 ppm), and the one corresponding to DG-H-DG moieties (pure form, δ 64.88 ppm), for P(BS-HDG)20 copolymer it is also possible to observe two peaks at δ 64.43 ppm and δ 64.03 ppm, corresponding to DG-B-S and S-B-DG sequences (mixed forms), in which butanediol is bound to a succinic subunit on one side and a diglycolic subunit on the other, respectively. It is also possible to note the signals related to DG-H-S and S-H-DG sequences (mixed forms), in which hexanediol is bound to the diglycolic subunit on one side and to the succinic subunit on the other, which fall at δ 64.91 ppm and δ 64.59 ppm. Last, in P(BS-HDG)120, peaks corresponding to DG-B-DG and S-H-S segments (inverted pure forms) are also observed at δ 64.32 ppm and δ 64.64 ppm, respectively.

The block length is defined as:

$$L_{B-S}=\frac{1}{P_{B-S}} \quad L_{H-DG}=\frac{1}{P_{H-DG}} \quad L_{B-DG}=\frac{1}{P_{B-DG}} \quad L_{H-S}=\frac{1}{P_{H-S}} \tag{1}$$

where $P_{B\text{-}S}$ and $P_{B\text{-}DG}$ are the probability of finding a butylene unit next to a succinic unit and the probability of finding a butylene unit next to a diglycolic one, respectively. $pH_{\text{-}DG}$ and $pH_{\text{-}S}$ correspond to the probability of finding a hexamethylene unit next to a diglycolic one and the probability of finding a hexamethylene unit next to a succinic one. These probabilities can be expressed as follows:

$$P_{B-S}=\frac{(I_{DG-B-S}+I_{S-B-DG})/2}{(I_{DG-B-S}+I_{S-B-DG})/2+I_{S-B-S}} P_{B-DG}=\frac{(I_{DG-B-S}+I_{S-B-DG})/2}{(I_{DG-B-S}+I_{S-B-DG})/2+I_{DG-B-DG}}$$
$$P_{H-DG}=\frac{(I_{S-H-DG}+I_{DG-H-S})/2}{(I_{S-H-DG}+I_{DG-H-S})/2+I_{DG-H-DG}} P_{H-S}=\frac{(I_{S-H-DG}+I_{DG-H-S})/2}{(I_{S-H-DG}+I_{DG-H-S})/2+I_{S-H-S}} \tag{2}$$

where $I_{DG\text{-}B\text{-}S}$, $I_{S\text{-}B\text{-}DG}$, $I_{S\text{-}H\text{-}DG}$ and $I_{DG\text{-}H\text{-}S}$ are the integrated intensities of the peaks related to DG-B-S, S-B-DG, S-H-DG and DG-H-S sequences, while $I_{S\text{-}B\text{-}S}$, $I_{DG\text{-}H\text{-}DG}$, $I_{DG\text{-}B\text{-}DG}$ and $I_{S\text{-}H\text{-}S}$ are the integrated intensities of

all the pure forms S-B-S, DG-H-DG, DG-B-DG and S-H-S, respectively. The intensities of all these integrals, as well as the probability values, calculated according to Eq. (2), are listed in Table S1.

The block length values of the copolymers studied are given in Table 1. As expected, the average block length decreases by increasing mixing time, reflecting the progress of the transesterification reactions.

From the probability values it is also possible to derive the degree of randomness (b), which can be defined as:

$$b = P_{B-S} + P_{B-DG} + P_{H-DG} + P_{H-S} \quad (3)$$

More in detail, in the case of a physical blend b is equal to 0, values of b between 0 and 1 indicate the presence of long blocks, b greater than 1 indicate the presence of shorter blocks, while a value of b equal to 2 means a statistical distribution of the sequences [42,43]. According to the data listed in Table 1 and in agreement with the values of block length, it can be seen that for P(BS-HDG)5 and P(BS-HDG)20 b is quite close to zero ($b = 0.12$ and 0.33, respectively), indicating a molecular architecture characterized by long blocks, reaching a value close to 2 for P(BS-HDG)120, typical of random copolymers.

The homopolymers and the three copolymers were then analysed through gel permeation chromatography. The values of molecular weight (M_n) and polydispersity index (Đ) are shown in Table 1: as can be seen, all the materials have a high molecular weight, of about 40,000 g/mol for PHDG and of about 77,000 g/mol for PBS, with a polydispersity index between 1.4 and 1.5, typical of polymers obtained by polycondensation. As expected, the copolymers show comparable values of molecular weight, in between those of the reference homopolymers. More in detail, a slight increase in molecular weight with mixing time was observed due to the fact that transesterification reactions prevail over chain scission ones at longer mixing times [44]. These results further confirm the good control of the synthetic process and the optimisation of the reaction conditions, which make it possible to rule out any effect of molecular weight on the properties described below.

3.2. Morphological characterisation

The cryo-fractured surface obtained from the physical blend PBS/PHDG and the P(BS-HDG)5 copolymer were subjected to morphological characterisation by SEM analysis (Fig. 3). Both the materials are characterised by a homogeneous and flat fracture surface with no significant voids or protrusions. This evidence, which was confirmed even at higher magnifications, indicates the good compatibility between PBS and PHDG both in the physical blend and in the copolymer, which is a necessary condition to obtain suitable functional properties.

3.3. Thermal and structural characterisation

All the compression moulded films were subjected to calorimetric analysis (DSC). The data for the first and second DSC scan are given in Table 2, while the corresponding plots are shown in Fig. 4.

As to the two homopolymers (Fig. 4A), they both exhibit a behaviour typical of semicrystalline materials. More specifically, in the case of PBS, a slight endothermic baseline jump relative to the glass-to-rubber transition can be observed at −32 °C, well below room temperature, indicating a mobile amorphous phase. At higher temperature (113 °C), an intense endothermic peak is observed, corresponding to melting of the crystalline fraction. As already mentioned, the high melting temperature of PBS is fundamental to ensure the presence of a *hard* phase in the copolymers, aiming to obtain a shape memory behaviour. PHDG also shows a T_g below T_{room}, at −39 °C, followed by an intense melting peak at 39 °C. The fact that this homopolymer melts at a much lower temperature than PBS, and just above room temperature, can be explained on the basis of a lower symmetry of its chains, due to the presence of ether-linkages, and ensures the presence of a *soft*, low-melting phase, which is necessary to impart a temporary shape.

As to the physical blend, only the T_g of PHDG is visible, the one of PBS, although present, being too small to be detected. Two T_ms, at 38 °C and 113 °C, ascribable to the crystalline phases of both PHDG and PBS homopolymers, respectively, were also observed. The intensity of the former peak is remarkably lower than the latter, indicating that crystallization capability of PHDG was quite depressed.

For the copolymers, only one glass transition is visible at intermediate temperatures with respect to that of the two reference homopolymers, and very similar to each other: this is not surprising given that PBS and PHDG have very similar glass transition temperatures. Moreover, two endothermic peaks are always present, indicating the semicrystalline nature of all the copolymers. As the mixing time increases and the block length decreases (Table 1), the higher melting peak, associated to PBS crystalline phase, moves towards lower temperatures until it converges with the lower endotherm, as in the case of P(BS-HDG)120. A parallel gradual decrease in ΔH_m, from 38.5 J/g for P(BS-HDG)5 to 11 J/g for P(BS-HDG)120, was also observed, indicating a progressive decrease of crystallinity of the samples. Moreover, the melting endotherms appear in all cases wider than those of the reference homopolymers, indicating the presence of crystallites with a wide distribution of degrees of perfection.

Following the first scan and a rapid cooling of the polymer melt, a second heating scan was performed, in order to minimise crystallisation phenomena and to observe the thermal behaviour of the materials as much independently as possible from their thermal history (Fig. 4B). In detail, PBS shows a behaviour similar to that observed in the first scan, indicating that the experimental conditions adopted were not sufficient to quench the material. Conversely, PHDG was successfully quenched, as it was completely amorphous, only the T_g jump being visible. The different crystallization capability of the two homopolymers is once again due to the lower symmetry of the chains in the ether-linkages containing polyester.

In the physical blend and in the copolymer with longer blocks, only the higher melting peak is visible, in agreement with what occurs in the two reference homopolymers. The copolymer with an intermediate block length, P(BS-HDG)20, shows a different crystallisation capacity: in particular, an exothermic crystallization peak is observed at 22 °C, in the temperature window between T_g and T_m, followed by an endothermic melting one at 85 °C. Since the heat associated with crystallisation (ΔH_c) is lower than that associated with melting (ΔH_m), it can be concluded that also this copolymer is semicrystalline. Lastly, the copolymer with shortest blocks (P(BS-HDG)120) shows only the endothermic jump associated with glass transition. As to the T_g values, they are all in line with those measured during the first scan.

To confirm that in the copolymers the tendency of PBS to crystallize decreases, all the samples were subjected to a controlled cooling rate from the melt. The exothermic crystallization peaks of the samples under investigation are displayed in Fig. S3: as it can be seen, PHDG and the random copolymer are unable to crystallize. Moreover, the temperature corresponding to the maximum of the exothermal crystallization peak (Table S2) regularly decreased from PBS to the blend and the copolymers, as the mixing time was increased, indicating that the crystallization becomes more difficult as the BS block length decreased. This evidence can be ascribed to the effect of the PHDG phase, which may act

Table 1
Molecular characterisation data (^{13}C NMR and GPC) of PBS, PHDG and the copolymers.

Samples	^{13}C NMR					GPC	
	L_{B-S}	L_{B-DG}	L_{H-DG}	L_{H-S}	b	M_n (g/mol)	Đ
PBS	-	-	-	-	-	76,700	1.4
P(BS-HDG)5	23	-	13	-	0.12	62,500	1.4
P(BS-HDG)20	6	-	6	-	0.33	67,100	1.4
P(BS-HDG)120	3	2	2	2	1.83	71,300	1.4
PHDG	-	-	-	-	-	40,400	1.5

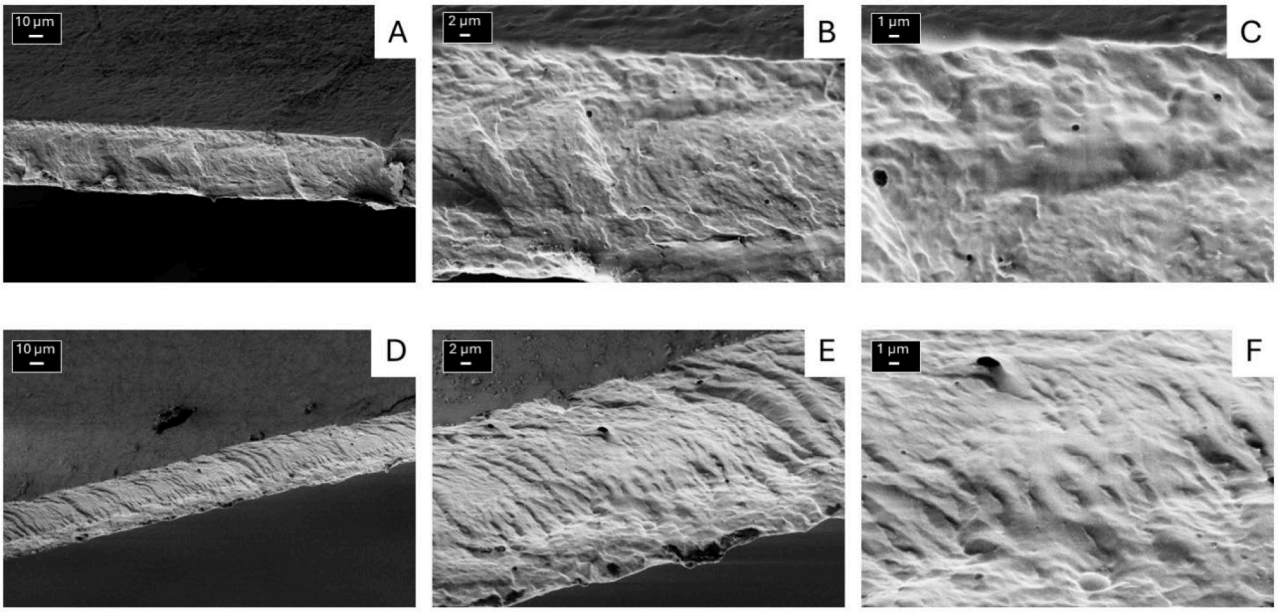

Fig. 3. SEM micrographs of cryo-fractured cross-sections of PBS/PHDG (A-B-C) and P(BS-HDG)5 (D-E-F) at different magnifications (A and D: 1000 x; B and E: 3500 x; C and F: 8000 x).

Table 2
Thermal (TGA and DSC) and structural (WAXS) characterization data of PBS, PHDG, PBS/PHDG and the copolymers.

Samples	TGA		DSC										WAXS
			I scan				II scan						
	T_{onset} (°C)	T_{max} (°C)	T_g (°C)	ΔC_p (J/g* °C)	T_m (°C)	ΔH_m (J/g)	T_g (°C)	ΔC_p (J/g* °C)	T_{cc} (°C)	ΔH_{cc} (J/g)	T_m (°C)	ΔH_m (J/g)	X_c (%)
PBS	372	399	−32	0.135	113	54	−32	0.121	-	-	113	50	34 ± 3
PHDG	365	388	−39	0.563	39	36	−39	0.753	-	-	-	-	30 ± 3
PBS/PHDG	368	394	−39	0.324	38	3	−39	0.449	-	-	112	36	28 ± 2
					113	39							
P(BS-HDG)5	365	396	−38	0.409	42	3	−38	0.491	-	-	111	37	26 ± 3
					110	36							
P(BS-HDG)20	372	397	−37	0.407	40	5	−37	0.465	22	19	85	38	18 ± 2
					84	27							
P(BS-HDG)120	370	397	−38	0.546	36	11	−38	0.497	-	-	-	-	5 ± 1

as a defect during chain folding.

Thermogravimetric Analysis (TGA) was carried out under inert atmosphere to verify the thermal stability of the materials. The TGA curves are shown in Fig. 4C, while the temperatures of onset (T_{onset}) and that corresponding to the maximum rate of weight loss (T_{max}) are given in Table 2. Thermal stability of all the samples is high and comparable, with T_{onset} above 360 °C and T_{max} above 385 °C. However, some differences can be observed: PBS homopolymer has the highest thermal stability with a T_{onset} of 372 °C and a T_{max} of 399 °C, while PHDG is the least stable, with a T_{onset} of 365 °C and a T_{max} of 388 °C, as a result of the presence of ether oxygen atoms along the macromolecular chain [38, 45]. As expected, the physical blend and the copolymers show intermediate values between those of the reference homopolymers. Looking at the degradation profiles, in all cases they are similar and overlapping, with a single step weight loss profile and a residual weight of about 5 %. In conclusion, the results obtained show that both the physical blending and the copolymerisation processes did not adversely affect the high thermal stability of the starting homopolymers.

The WAXS diffraction profiles of the obtained samples are shown in Fig. 4D, while the values of degree of crystallinity (X_c) are given inTable 2.

The diffractograms of all the samples are typical of semicrystalline materials, in agreement with calorimetric data (Fig. 4A): the profiles show some reflections due to the ordered part of the material, superimposed on a bell-shaped baseline due to the amorphous phase. Both homopolymers are characterised by a pronounced and similar crystallinity, with clear and rather narrow reflections, indicating crystalline phases with a good degree of perfection. The diffraction profiles of the blend and of P(BS-HDG)5 clearly show the diffraction peaks of the two reference homopolymers, while in the copolymer characterized by shorter blocks all the peaks become wider and less intense, with a profile similar to that of PBS (see the guides for the eye in Fig. 4D), confirming that at longer mixing times only the crystalline phase of this homopolymer could develop. Looking at the calculated X_c values (Table 2), it can be confirmed that longer copolymerisation times lead to a progressive decrease in the degree of crystallinity, reaching values of only 5 % for P(BS-HDG)120 copolymer. All these results are in line with calorimetric data.

3.4. Mechanical characterisation

To evaluate the mechanical performances of the materials under study, tensile mechanical tests were performed. The obtained values of Young's modulus (E), stress (σ_b) and strain (ε_b) at break are listed in Table 3, while the relative stress-strain curves are shown in Fig. 5.

PBS proved to be the most rigid material among those tested, with

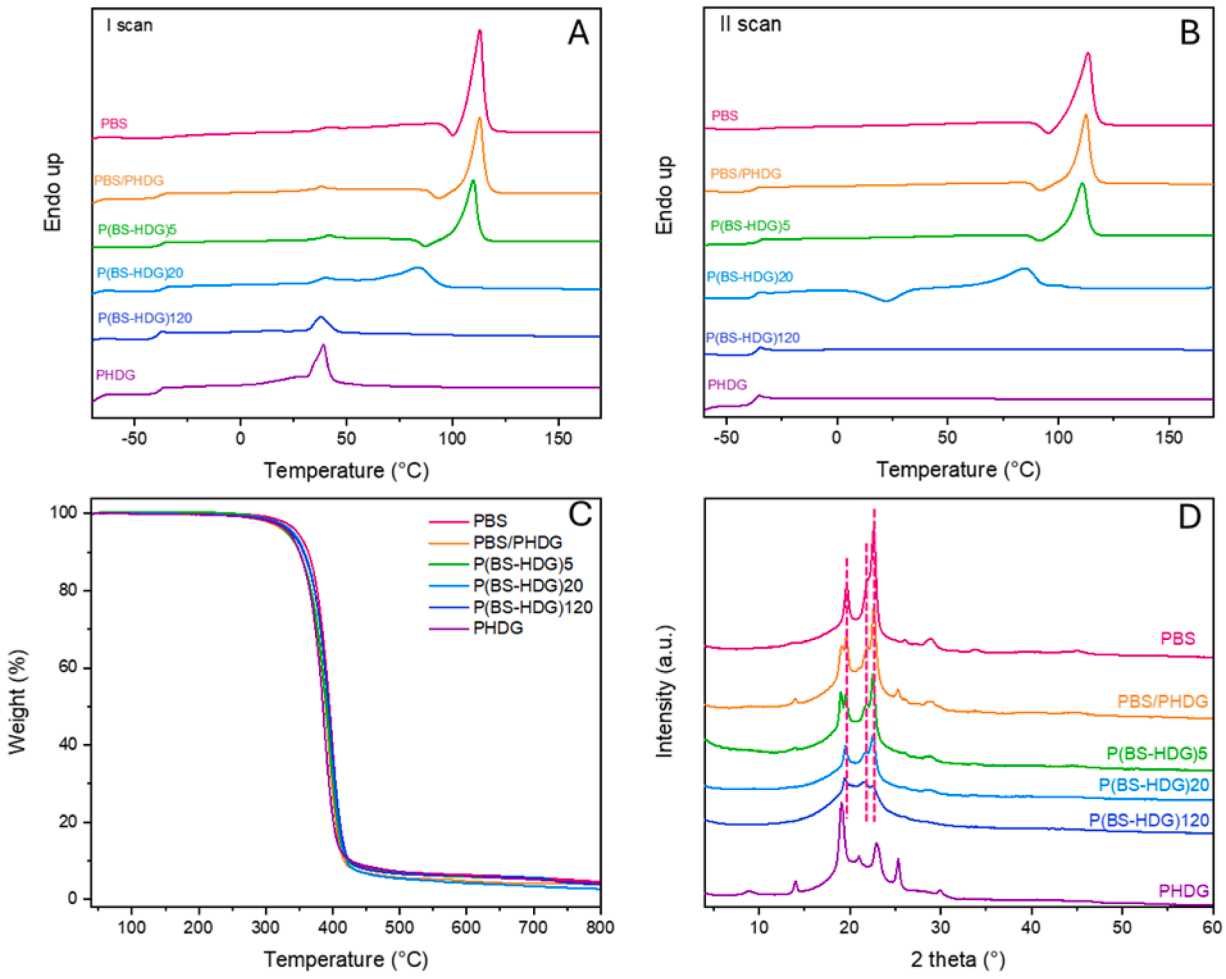

Fig. 4. First (A) and second (B) DSC scans, TGA curves (C) and WAXS profiles (D) of PBS, PHDG, PBS/PHDG and copolymers.

Table 3
Mechanical characterization data of PBS, PHDG, PBS/PHDG and copolymers.

Samples	E (MPa)	σ_b (MPa)	ε_b (%)
PBS	447 ± 23	29 ± 3	14 ± 2
PBS/PHDG	122 ± 15	8 ± 1	49 ± 27
P(BS-HDG)5	108 ± 14	9 ± 1	120 ± 63
P(BS-HDG)20	107 ± 10	10 ± 2	636 ± 33
P(BS-HDG)120	8 ± 2	1.7 ± 0.5	560 ± 145
PHDG	73 ± 23	3.3 ± 0.6	34 ± 10

the highest values of Young's modulus (447 MPa) and stress at break (29 MPa) and the lowest elongation at break (14 %). PHDG, on the other hand, has lower values for modulus and elongation at break, of 73 and 3 MPa respectively, and a rather low elongation at break, of about 35 %. Quite surprisingly, both the physical blend and all the copolymers are characterized by better elongations compared to the reference homopolymers. More in detail, PBS/PHDG shows an intermediate behaviour in terms of elastic modulus and stress at break, with an elongation at break of >80 %. This result can be explained in terms of the good compatibility between the two homopolymers, as confirmed by SEM analysis (Fig. 3).

Regarding the copolymers, the presence of ether oxygen atoms in the macromolecular chain causes a significant change in the mechanical response compared to PBS, resulting in a general decrease of the values of E and σ_b together with a parallel increase of ε_b, as already studied in the literature [45–47]. More in detail, in both the copolymers with longer blocks, there is a similar and remarkable decrease in Young's modulus and in the stress at break compared to those observed for PBS, regardless of the length of the blocks. Conversely, the two copolymers significantly differ in their elongation at break, which was of 152 % for P(BS-HDG)5 and of 636 % for P(BS-HDG)20. The random copolymer, on the other hand, has the lowest values of both Young's modulus and stress at break among all the materials studied, together with and an excellent elongation at break, of 560 %.

The overall trend cannot be ascribed to the polymer molecular weights, which were all high and comparable (Table 1), or to chain flexibility, as all the T_g values are similar and well below room temperature (Table 2). Conversely, it can be noticed that the mechanical flexibility becomes higher as the block length and, in turn, the crystallinity degree, decrease.

Finally, it is interesting to note that the stress-strain curves of PBS/PHDG, P(BS-HDG)5 and P(BS-HDG)120 did not show any yield. Therefore, to evaluate their elastomeric properties, the two materials suitable for use as memory shape polymers, PBS/PHDG and P(BS-HDG)5, were therefore subjected to cyclic tests. Fig. 5B and 5C show the relative curves, while in Table S3 cyclic tests data are listed. As expected, lower strains result in a slightly higher percentage of shape recovery, which was approximately 63 % for PBS/PHDG and 71 % for P(BS-HDG)5. For the highest elongation, the recovery is approximately 56 % for the blend and 63 % for the copolymer. Moreover, the recovery for the copolymer is slightly higher than for the physical blend for both deformations, as a result of the presence of chemical bonds between the two components instead of only physical interactions as in the case of the blend. Hysteresis, which was evaluated on the twenty-first cycle, slightly increases with deformation, rising from values of 3.4 and 1.7 for

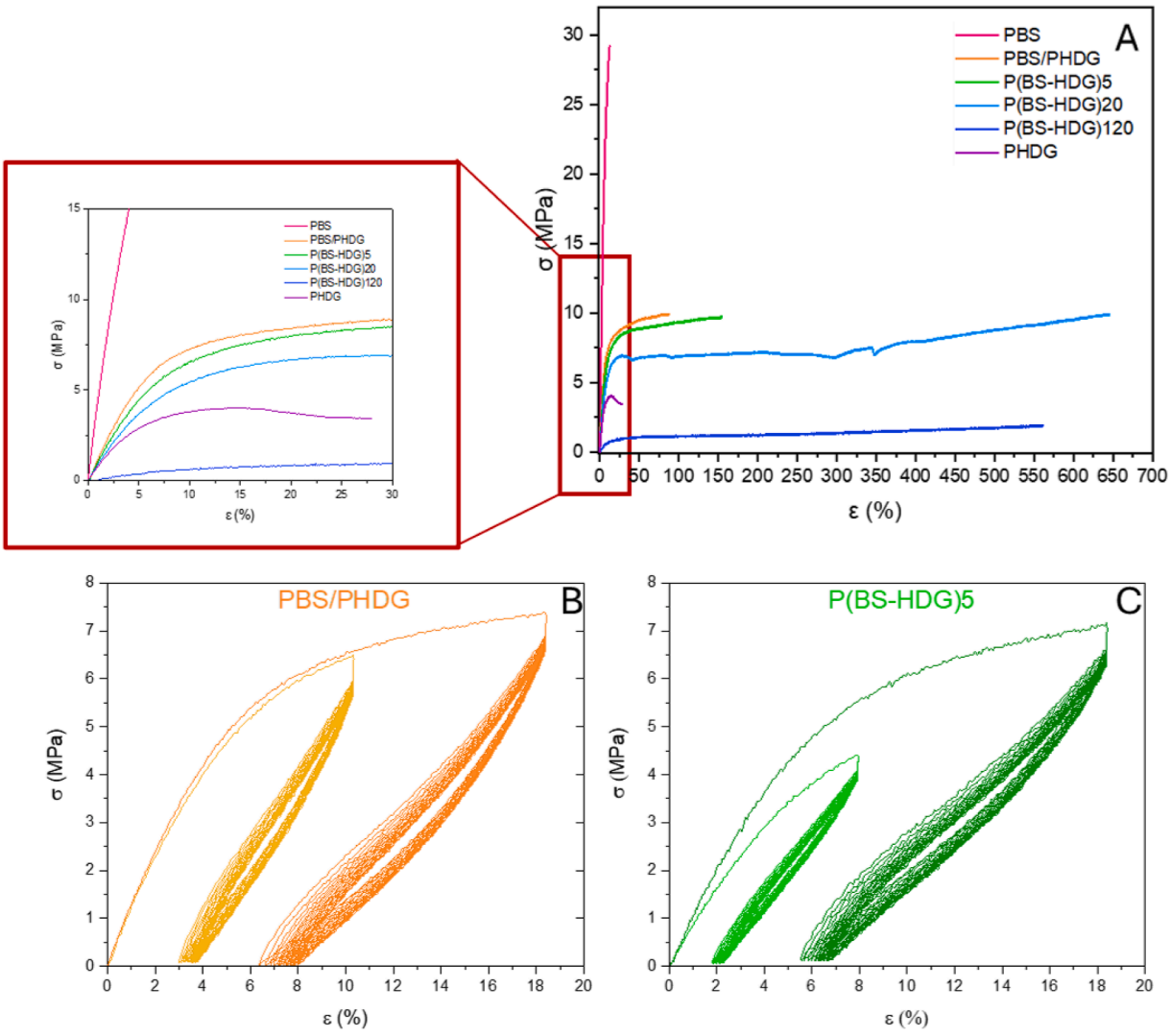

Fig. 5. A) Stress–strain curves of the samples under study. In the insert: magnification of the curves at low strain values; Stress–strain curves obtained from cyclic testing of B) PBS/PHDG at 8 % and 18 % of maximum elongation and C) P(BS-HDG)5 at 10 % and 20 % of maximum elongation.

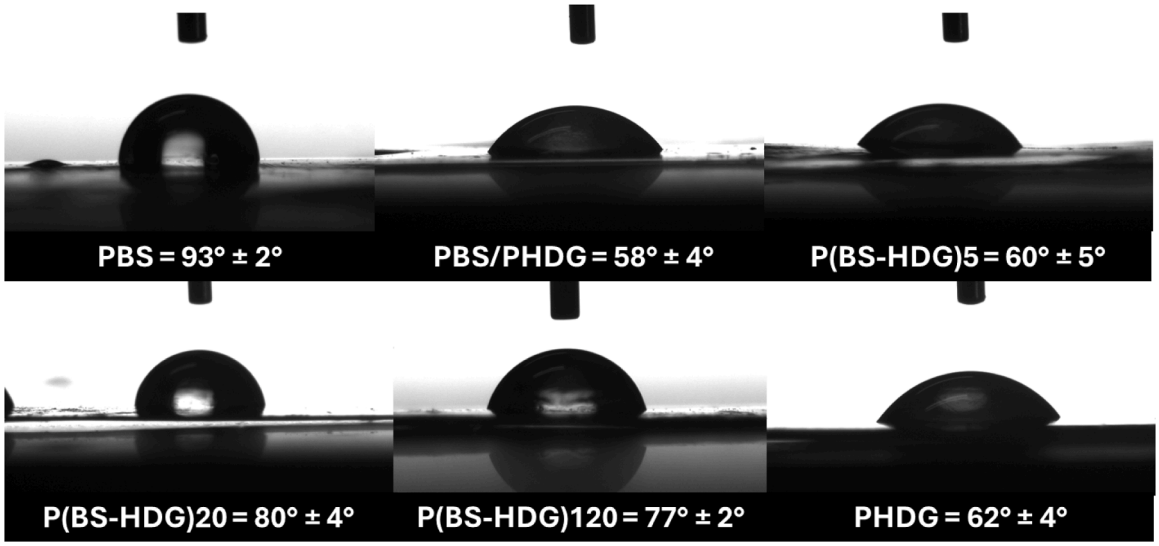

Fig. 6. Images of water droplets immediately after deposition on film surfaces of PBS, PHDG, PBS/PHDG and copolymers.

PBS/PHDG and P(BS-HDG)5 to around 5–6 mJ/mm^3 in both the cases.

3.5. Surface wettability measurements

Surface wettability measurements were carried out to evaluate the surface hydrophilicity of the polymer films. In Fig. 6 the profiles of different droplets deposited on the films are shown and the values of water contact angle (WCA) are listed.

As can be seen, PBS shows a hydrophobic behaviour, with the highest WCA value among the family (WCA = 93°), while PHDG is hydrophilic, with a contact angle of about 62°, due to the presence of ether oxygens atoms along its macromolecular chain [38,46]. In general, the blend and the three copolymers are characterised by a hydrophilic behaviour, with WCA values intermediate between those of the homopolymers. However, some important differences, due to the different block lengths, can be observed. In particular, the physical blend and the copolymer with longest blocks show WCA values similar to those of PHDG, while the other two copolymers have a surface wettability more similar to that of PBS. This result could be explained by the assumption of a rapid spatial reorganisation of the chains in contact with water, bringing the more hydrophilic HDG segments towards the surface, resulting in lower WCA values. This surface reorganisation, which has been already documented in the literature [48], is most effective when the chains are mobile at room temperature and only when the hydrophilic segments are sufficiently long, as in the case of PBS/PHDG and P(BS-HDG)5.

3.6. Functional characterisation

Preliminary shape memory evaluation, hydrolytic degradation tests and *in-vitro* cytotoxicity studies, were carried out only on the blend and the copolymer with longest blocks, as these two materials exhibit the fundamental thermal characteristics of shape memory materials and the proper mechanical response.

Qualitative shape memory evaluation

Fig. 7 shows a schematic illustration of the thermal shape memory process, followed by an example of the qualitative test conducted on the PBS/PHDG blend.

As to the qualitative evaluation of their shape memory behaviour, first, linear strips obtained from PBS/PHDG and P(BS-HDG)5 were given a temporary spiral shape and they were then immersed in water maintained at a temperature of 60 °C. It was observed that both strips immediately recovered the original form, confirming their shape memory behaviour. The immediacy of the switch between the temporary and permanent forms can be seen in the video (see supplementary material) showing the experiment conducted on P(BS-HDG)5.

Hydrolytic degradation tests

PBS/PHDG and P(BS-HDG)5 films were subjected to in vitro hydrolytic degradation experiments under physiological temperature (37 °C) and pH (7.4), in order to evaluate their applicability as bioresorbable materials. PBS homopolymer was also tested, for sake of comparison, while PHDG was excluded from this analysis because 37 °C was too close to its melting temperature (Table 2).

First, gravimetric weight loss measurements were performed on the partially degraded samples and on their relative blanks as a function of incubation time (Fig. 8A). As expected, the gravimetric weights of all the blanks remain practically unchanged over time (data not shown). The same behaviour was observed for PBS homopolymer, in line with literature data [31,32,49,50]. Conversely, blending and copolymerization with PHDG results in a significant weight loss, which increases with incubation time. Moreover, in the early stages of the process (up to 3 months), weight loss is not significant, as the macromolecules formed by the hydrolysis reactions are not short enough to diffuse through the polymer matrix and penetrate into solution. As the hydrolysis process proceeds, short water-soluble sequences are formed, and gravimetric weight changes become significant [48].

Comparing the different samples after 6 months of incubation, it can be seen that the blend is characterised by weight loss of about 20 %, which is slightly lower than the one obtained for the block copolymer, of about 33 %. As known degradation occurs faster for amorphous, rubbery and hydrophilic samples, as all these features make the material more accessible to water attack [51,52]. In the preset case, considering that the two samples are characterized by similar chain mobility, crystallinity degree and surface wettability, a possible explanation can be found taking into account that the long HDG blocks inside the copolymer may form shorter oligomers than those generated from neat PHDG homopolymer inside the physical blend.

The percentage molecular weight loss has been also calculated for PBS and P(BS-HDG)5 copolymer, and the obtained values are reported in Fig. 8B, as a function of time. As it can be seen, PBS undergoes only a slight molecular weight loss, increasing with incubation time, up to 21 % after 180 days. The presence of ether oxygen atoms in P(BS-HDG)5 copolymer results in a significant molecular weight loss, which was of about 65 % at the end of the experiment, in line with what already observed for gravimetric weight loss. Although it was impossible to calculate the M_n values for the blend, the relative chromatograms at the same timepoints are shown in Figure S4. As it can be observed, the chromatogram of the neat blend is characterized by a wide peak, resulting from the overlapping of the chromatograms of the two reference homopolymers, with a maximum at a retention time of about 6 min. As to partially degraded samples, an evolution of both peak profile and position was observed by increasing the incubation times. More in detail, the chromatograms were progressively shifted towards the region corresponding to lower molecular weights (i.e. higher retention times), while multiple shoulders became visible and progressively more

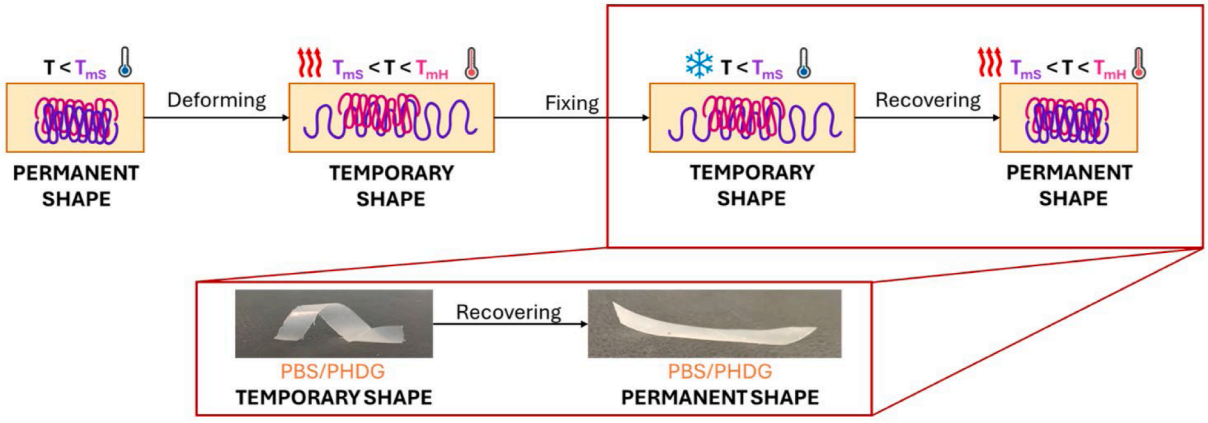

Fig. 7. Schematic illustration of shape memory process and qualitative shape memory test on PBS/PHDG film.

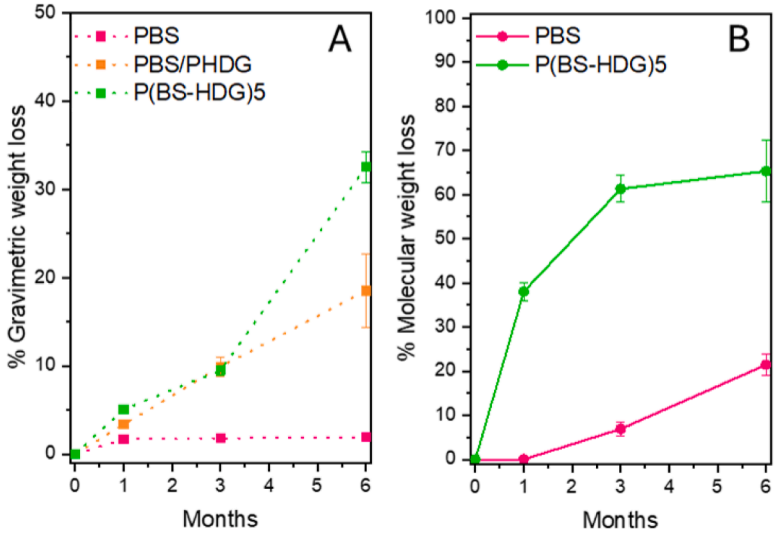

Fig. 8. A) Gravimetric weight loss and B) molecular weight loss as a function of incubation time of PBS, PBS/PHDG and P(BS-HDG)5.

pronounced at higher retention times. This result confirms the formation of low molecular weight chains, which become progressively shorter as the incubation time is increased.

In order to verify how the degradation process might have affected the main thermal transitions of the materials under investigation, I DSC scans were carried out on partially degraded samples, and on the relative blanks (Fig. S5, Table S4).

For PBS homopolymer, it is possible to observe only a similar and slight increase in crystallinity (higher melting enthalpy) in blank samples compared to the neat film, due to annealing at 37 °C. As to partially degraded samples, this phenomenon becomes more evident over time, indicating also a partial hydrolytic attack of amorphous regions,

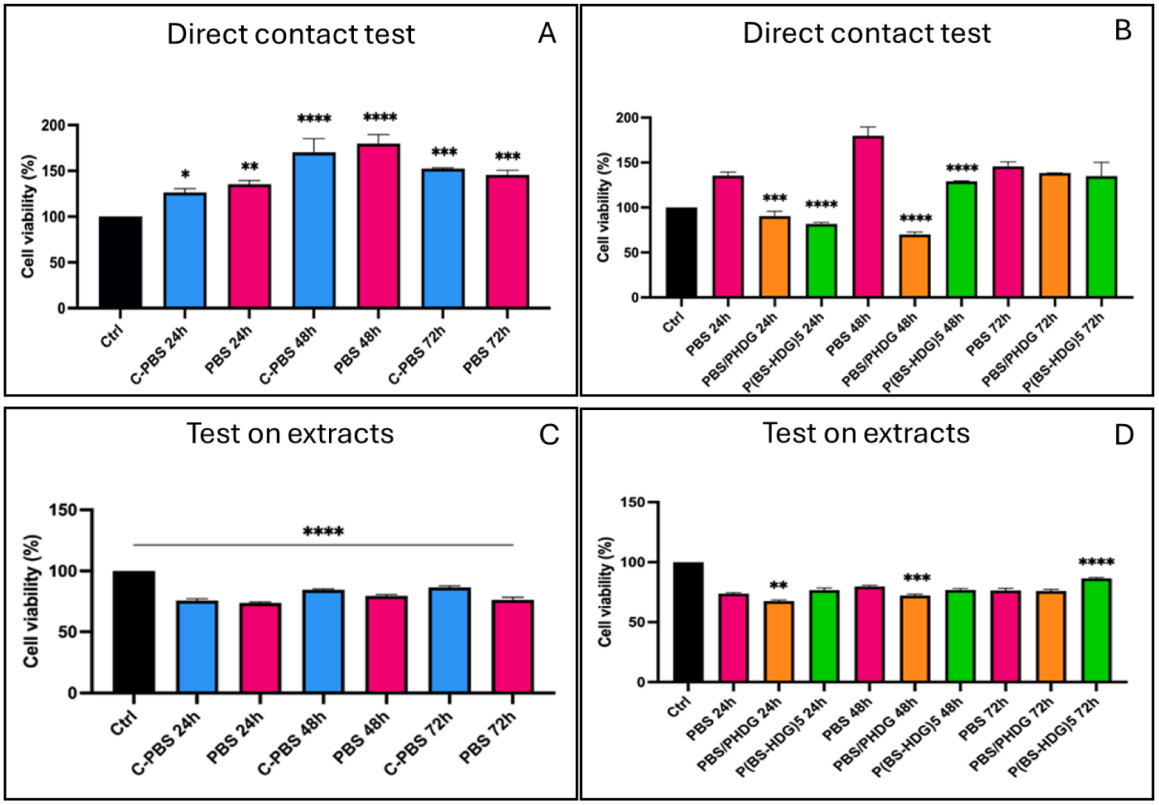

Fig. 9. Cytotoxicity tests suggested by ISO 10,993–5 expressed as percentage of cell viability ± SD. A) Direct contact test of commercial PBS (C-PBS) and synthetised (PBS). Data were expressed in percentage and normalised to untreated controls at 24, 48 and 72 h and analysed by One-way Anova test with Dunnett's multiple comparison (* $p < 0.05$; ** $p < 0.01$; *** $p < 0.001$; **** $p < 0.0001$) and B) direct contact test between PBS/PHDG and P(BS-HDG)5 compared to PBS as material control analysed by One-way Anova test with Bonferroni's multiple comparison (***$p < 0.0002$,****$p < 0.0001$). C) Test on extracts of commercial PBS (C-PBS) and synthetized (PBS). Data were expressed in percentage and normalised to untreated controls at 24, 48 and 72 h and analysed by One-way Anova test with Dunnett's multiple comparison (* $p < 0.05$; ** $p < 0.01$; *** $p < 0.001$; **** $p < 0.0001$) and D) test on PBS/PHDG and P(BS-HDG)5 extracts compared to PBS extract as material control analysed by One-way Anova test with Bonferroni's multiple comparison (** $p < 0.001$,***$p < 0.0003$,****$p < 0.0001$).

resulting from incubation in phosphate buffer.

As to PBS/PHDG and P(BS-HDG)5, comparing the neat samples with the corresponding blanks at different incubation times, it can be observed that the highest melting peak, related to the melting of the crystalline phase of PBS, becomes slightly more intense, due to annealing phenomena. The smaller endothermic peaks, visible in the neat samples at a temperature between 38 and 40 °C, apart from slightly increasing in intensity, move also towards higher temperatures, indicating that the permanence at 37 °C favours the formation of a higher amount of more perfect crystals.

On the other hand, in the case of the partially degraded PBS/PHDG films, an initial splitting of the lower melting peaks is observed, which returns to a single signal at slightly higher temperatures after 3 months, due to the degradation of less perfect crystals. As to the melting peak ascribable to the crystalline phase of PBS, the same trend already observed for incubated PBS samples was noticed. In the case of the P(BS-HDG)5 copolymer, the melting peak relative to the lower melting component disappears after 6 months, indication of complete degradation of these less perfect crystals. As in the previous case, the melting peak relative to the PBS fraction increases in intensity, indicating a higher degree of crystallinity.

In-vitro cytotoxicity tests

To assess the cytotoxic potential of the tested polymers, phCornF cells were cultured in direct contact with the materials, and cell viability was evaluated using the MTT assay at 570 nm after 24, 48, and 72 h of incubation. As shown in Fig. 9A, cells exposed to both commercial PBS and PBS synthesised in the present work (C-PBS and PBS, respectively) exhibited viability levels comparable to those of the untreated control group after 24 h. Notably, a progressive increase in cell viability was observed after 48 h, indicating a time-dependent enhancement in cell metabolic activity. These findings suggest that PBS does not induce cytotoxic effects under the tested conditions and may be considered a suitable negative control material in biocompatibility studies.

Direct contact test was assessed also to evaluate the preliminary cytotoxicity of PBS/PHDG and P(PBS-HDG)5 compared with control (Fig. 9B). After 24 h, cells in contact with PBS/PHDG and P(PBS-HDG)5 displayed a lower viability compared to PBS. A similar trend was observed at 48 h: PBS maintained high cell viability, while PBS/PHDG and P(PBS-HDG)5 exhibited a decreased metabolic activity. Last, at 72 h, cell viability improved across all groups. Therefore, despite the initial reduction in viability, both polymer-exposed groups increased their viability over time compared to PBS, all the experimental groups showing >70 % viability in correspondence to the longer timepoint. This suggests a potential time-dependent cell adaptation and viability, as well as a low impact of the materials studied on cell survival for longer times.

Cells were also exposed to copolymer extracts in order to evaluate the release of toxic substances. All the experimental groups showed >70 % cell viability compared to the control (Fig. 9C) and to PBS (Fig. 9D). Last, after 72 h of incubation, viability exhibited by cells cultured with extracts obtained from the copolymer was significatively higher than the one observed for cells in presence of other extracts.

4. Conclusions

Biomaterials are playing an increasingly important role in the biomedical sector, particularly in emerging and innovative fields such as ophthalmic and corneal microsurgery. Given the delicate nature of this type of surgery, polymers — especially aliphatic polyesters — have proven to be the most interesting class of materials in this regard. Accordingly, this work reports on various successful strategies for chemically and physically modifying poly(butylene succinate), an aliphatic polyester with proven biocompatibility but characterised by excessive rigidity for the manufacture of ophthalmic devices and a limited degradation rate. A physical blend was prepared and copolymers with a different molecular architecture have been synthesised by introducing, into the PBS macromolecular chain, the same weight percentage of poly(hexamethylene diglycolate), PHDG. This last was chosen due to the presence of ether oxygen atoms, which are known to reduce crystallinity, increase wettability and flexibility, and speed up degradation in a hydrolytic environment. All the obtained materials showed tuneable crystallinity, hydrophilicity and mechanical properties, depending on block length. Moreover, from cyclic tests performed on the physical blend and the copolymer with the longest blocks a good recovery was also observed. In terms of hydrolytic degradation rate, the results were very promising: the biodegradability of PBS increased through copolymerisation and mixing. Although qualitatively evaluated, the ambitious goal of realising shape memory materials was also achieved. Lastly, it should be noted that the biocompatibility of PBS has been preserved, as confirmed by cytotoxicity tests, which showed a high corneal cells viability. All these evidences confirmed the preliminary suitability of the investigated polymeric system for potential application as shape-memory sutures in the field of corneal surgery.

CRediT authorship contribution statement

Arianna Palumbo: Writing – review & editing, Writing – original draft, Validation, Investigation, Formal analysis, Data curation. **Gloria Astolfi:** Writing – original draft, Investigation, Formal analysis, Data curation. **Michelina Soccio:** Writing – review & editing, Validation, Formal analysis. **Giulia Guidotti:** Writing – review & editing, Writing – original draft, Validation, Methodology, Data curation. **Elisa Boanini:** Investigation, Formal analysis, Data curation. **Elisabetta Salatelli:** Investigation, Formal analysis. **Piera Versura:** Validation, Supervision. **Nadia Lotti:** Validation, Supervision, Resources, Project administration, Funding acquisition, Conceptualization.

Declaration of competing interest

The authors declare that they have no known competing financial interests or personal relationships that could have appeared to influence the work reported in this paper.

Supplementary materials

Supplementary material associated with this article can be found, in the online version, at doi:10.1016/j.polymdegradstab.2025.111778.

Data availability

Data will be made available on request.

References

[1] A.W. Lloyd, R.G.A. Faragher, S.P. Denyer, Ocular biomaterials and implants, Biomaterials 22 (2001) 769–785, https://doi.org/10.1016/S0142-9612(00)00237-4.

[2] Y. Guo, V. Kratky, H. Xie, X. Shentu, X. Man, Y. Wang, W. Wen, A.C. Rokohl, L. M. Heindl, Grand Challenges and opportunities in surgical ophthalmology: together for a shared future, Front. Ophthalmol 2 (2022), https://doi.org/10.3389/fopht.2022.922240.

[3] WHO, Blind. vis. impair., (2023). https://www.who.int/news-room/fact-sheets/detail/blindness-and-visual-impairment.

[4] E.Y. Wang, X. Kong, M. Wolle, N. Gasquet, J. Ssekasanvu, S.P. Mariotti, R. Bourne, H. Taylor, S. Resnikoff, S. West, Global trends in blindness and vision impairment resulting from corneal opacity 1984–2020, Ophthalmology 130 (2023) 863–871, https://doi.org/10.1016/j.ophtha.2023.03.012.

[5] S.R. Flaxman, R.R.A. Bourne, S. Resnikoff, P. Ackland, T. Braithwaite, M. V. Cicinelli, A. Das, J.B. Jonas, J. Keeffe, J.H. Kempen, J. Leasher, H. Limburg, K. Naidoo, K. Pesudovs, A. Silvester, G.A. Stevens, N. Tahhan, T.Y. Wong, H. R. Taylor, R. Bourne, P. Ackland, A. Arditi, Y. Barkana, B. Bozkurt, T. Braithwaite, A. Bron, D. Budenz, F. Cai, R. Casson, U. Chakravarthy, J. Choi, M.V. Cicinelli, N. Congdon, R. Dana, R. Dandona, L. Dandona, A. Das, I. Dekaris, M. Del Monte, J. Deva, L. Dreer, L. Ellwein, M. Frazier, K. Frick, D. Friedman, J. Furtado, H. Gao, G. Gazzard, R. George, S. Gichuhi, V. Gonzalez, B. Hammond, M.E. Hartnett, M. He, J. Hejtmancik, F. Hirai, J. Huang, A. Ingram, J. Javitt, J. Jonas, C. Joslin, J. Keeffe, J. Kempen, M. Khairallah, R. Khanna, J. Kim, G. Lambrou, V.C. Lansingh, P. Lanzetta, J. Leasher, J. Lim, H. Limburg, K. Mansouri, A. Mathew, A. Morse, B. Munoz, D. Musch, K. Naidoo, V. Nangia, M. Palaiou, M.B. Parodi, F.Y. Pena,

K. Pesudovs, T. Peto, H. Quigley, M. Raju, P. Ramulu, Z. Rankin, S. Resnikoff, D. Reza, A. Robin, L. Rossetti, J. Saaddine, M. Sandar, J. Serle, T. Shen, R. Shetty, P. Sieving, J.C. Silva, A. Silvester, R.S. Sitorus, D. Stambolian, G. Stevens, H. Taylor, J. Tejedor, J. Tielsch, M. Tsilimbaris, J. Van Meurs, R. Varma, G. Virgili, Y.X. Wang, N.-L. Wang, S. West, P. Wiedemann, T. Wong, R. Wormald, Y. Zheng, Global causes of blindness and distance vision impairment 1990–2020: a systematic review and meta-analysis, Lancet Glob. Health 5 (2017) e1221–e1234, https://doi.org/10.1016/S2214-109X(17)30393-5.

[6] World Health Organization, World Report On vision, World Health Organization, Geneva, 2019. https://iris.who.int/handle/10665/328717 (accessed July 4, 2025).

[7] L. Ung, N.R. Acharya, T. Agarwal, E.C. Alfonso, B. Bagga, P.J. Bispo, M.J. Burton, J. K. Dart, T. Doan, S.M. Fleiszig, P. Garg, M.S. Gilmore, D.C. Gritz, L.D. Hazlett, A. Iovieno, V. Jhanji, J.H. Kempen, C.S. Lee, T.M. Lietman, T.P. Margolis, S. D. McLeod, J.S. Mehta, D. Miller, E. Pearlman, L. Prajna, N.V. Prajna, G. D. Seitzman, S.S. Shanbhag, N. Sharma, S. Sharma, M. Srinivasan, F. Stapleton, D. T. Tan, R. Tandon, H.R. Taylor, E.Y. Tu, S.S. Tuli, R.B. Vajpayee, R.N. Van Gelder, S.L. Watson, M.E. Zegans, J. Chodosh, Infectious corneal ulceration: a proposal for neglected tropical disease status, Bull. World Health Organ. 97 (2019) 854–856, https://doi.org/10.2471/BLT.19.232660.

[8] J.P. Whitcher, M. Srinivasan, M.P. Upadhyay, Corneal blindness: a global perspective, (n.d.).

[9] M. Park, A. Richardson, N. Delic, K. Nguyen, J. Biazik, R. Zhang, L. Sprogyte, L. Nureen, J. Lees, A. Fajardo, U. Kunicki, S.L. Watson, J. Males, N.D. Girolamo, A bioengineering-regenerative medicine approach for ocular surface reconstruction using a functionalized native cornea-derived bio-scaffold, Adv. Funct. Mater. 33 (2023) 2304856, https://doi.org/10.1002/adfm.202304856.

[10] L. Pagano, H. Shah, O. Al Ibrahim, K.A. Gadhvi, G. Coco, J.W. Lee, S.B. Kaye, H. J. Levis, K.J. Hamill, F. Semeraro, V. Romano, Update on suture techniques in corneal transplantation: a systematic review, J. Clin. Med. 11 (2022) 1078, https://doi.org/10.3390/jcm11041078.

[11] L.F.F. Smith, C.E. Hugkulstone, Long-term survival of corneal sutures: mersilene vs Nylon, Eur. J. Implant Refract. Surg. 6 (1994) 348–350, https://doi.org/10.1016/s0955-3681(13)80210-9.

[12] D. Landau, C.S. Siganos, H. Mechoulam, A. Solomon, J. Frucht-Pery, Astigmatism after mersilene and nylon suture use for penetrating keratoplasty, Cornea 25 (2006) 691–694, https://doi.org/10.1097/01.ico.0000208821.32614.49.

[13] M.C. Bartels, J. Van Rooij, A.J.M. Geerards, P.G.H. Mulder, L. Remeijer, Comparison of complication rates and postoperative astigmatism between Nylon and Mersilene sutures for corneal transplants in patients with Fuchs endothelial dystrophy, Cornea 25 (2006) 533–539, https://doi.org/10.1097/01.ico.0000214218.60249.e5.

[14] R. Lee, Georgiou Lam, Then Paul, I. Mavrikakis, C. Liu, Avadhanam, Suturing techniques and postoperative management in penetrating keratoplasty in the United Kingdom, Clin. Ophthalmol. (2012) 1335, https://doi.org/10.2147/opth.s35460.

[15] V.C. Brücher, N. Eter, C.E. Uhlig, Results of resorbable and running sutured amniotic multilayers in sterile deep corneal ulcers and perforations, Cornea 39 (2020) 952–956, https://doi.org/10.1097/ICO.0000000000002303.

[16] S.M. Bar-Sela, O. Spierer, A. Spierer, Suture-related complications after congenital cataract surgery: vicryl versus Mersilene sutures, J. Cataract Refract. Surg. 33 (2007) 301–304, https://doi.org/10.1016/j.jcrs.2006.10.039.

[17] H.S. Eustis, T.R. Elmer, G. Ellis, Postoperative results of absorbable, subconjunctival adjustable sutures, J. Am. Assoc. Pediatr. Ophthalmol. Strabismus 8 (2004) 240–242, https://doi.org/10.1016/j.jaapos.2004.01.013.

[18] C.E. Uhlig, V.C. Müller, Resorbable and running suture for stable fixation of amniotic membrane multilayers: a useful modification in deep or perforating sterile corneal ulcers, Am. J. Ophthalmol. Case Rep. 10 (2018) 296–299, https://doi.org/10.1016/j.ajoc.2018.04.012.

[19] Y. Yang, M. Chihaia, C.B. Schulz, A. Kenchington, B. Parkin, H. MacLean, 8-0 polyglactin 910 suture in entropion repair: long term follow up and rates of recurrence, Eye 37 (2023) 618–623, https://doi.org/10.1038/s41433-022-01997-5.

[20] Classical (Open) surgery, Biomed. Eng. Gastrointest. Surg. (2017) 221–267, https://doi.org/10.1016/b978-0-12-803230-5.00006-3.

[21] C.K.S. Pillai, C.P. Sharma, Review paper: absorbable polymeric surgical sutures: chemistry, production, properties, biodegradability, and performance, J. Biomater. Appl. 25 (2010) 291–366, https://doi.org/10.1177/0885328210384890.

[22] C.M. Hussain, S. Thomas, Polymers in biomedical use, Handb. Polym. Ceram. Nanotechnol (2021), https://doi.org/10.1007/978-3-030-40513-7_74.

[23] V.A. Zhukovskii, Problems and prospects for development and production of surgical suture materials, Fibre Chem. 40 (2008) 208–216, https://doi.org/10.1007/s10692-008-9039-0.

[24] C. Dennis, S. Sethu, S. Nayak, L. Mohan, Y.Yos Morsi, G. Manivasagam, Suture materials — Current and emerging trends, J. Biomed. Mater. Res. A 104 (2016) 1544–1559, https://doi.org/10.1002/jbm.a.35683.

[25] Y. Li, Q. Meng, S. Chen, P. Ling, M.A. Kuss, B. Duan, S. Wu, Advances, challenges, and prospects for surgical suture materials, Acta Biomater. 168 (2023) 78–112, https://doi.org/10.1016/j.actbio.2023.07.041.

[26] C. Liu, H. Qin, P.T. Mather, Review of progress in shape-memory polymers, J. Mater. Chem. 17 (2007) 1543, https://doi.org/10.1039/b615954k.

[27] C. Liu, S.B. Chun, P.T. Mather, L. Zheng, E.H. Haley, E.B. Coughlin, Chemically cross-linked polycyclooctene: synthesis, characterization, and shape memory behavior, Macromolecules 35 (2002) 9868–9874, https://doi.org/10.1021/ma021141j.

[28] J. Delaey, P. Dubruel, S. Van Vlierberghe, Shape-memory polymers for biomedical applications, Adv. Funct. Mater. 30 (2020), https://doi.org/10.1002/adfm.201909047.

[29] P.T. Mather, X. Luo, I.A. Rousseau, Shape memory polymer research, Annu. Rev. Mater. Res. 39 (2009) 445–471, https://doi.org/10.1146/annurev-matsci-082908-145419.

[30] M. Behl, J. Zotzmann, A. Lendlein, Shape-memory polymers and Shape-changing polymers, Adv Polym Sci. 226 (2009) 1–40, https://doi.org/10.1007/12200926.

[31] F. Cristofaro, M. Gigli, N. Bloise, H. Chen, G. Bruni, A. Munari, L. Moroni, N. Lotti, L. Visai, Influence of the nanofiber chemistry and orientation of biodegradable poly (butylene succinate)-based scaffolds on osteoblast differentiation for bone tissue regeneration, Nanoscale 10 (2018) 8689–8703, https://doi.org/10.1039/c8nr00677f.

[32] M. Fabbri, G. Guidotti, M. Soccio, N. Lotti, M. Govoni, E. Giordano, M. Gazzano, R. Gamberini, B. Rimini, A. Munari, Novel biocompatible PBS-based random copolymers containing PEG-like sequences for biomedical applications: from drug delivery to tissue engineering, Polym. Degrad. Stab. 153 (2018) 53–62, https://doi.org/10.1016/j.polymdegradstab.2018.04.011.

[33] G. Guidotti, M. Soccio, M. Gazzano, N. Bloise, G. Bruni, A. Aluigi, L. Visai, A. Munari, N. Lotti, Biocompatible PBS-based copolymer for soft tissue engineering: introduction of disulfide bonds as winning tool to tune the final properties, Polym. Degrad. Stab. 182 (2020) 109403, https://doi.org/10.1016/j.polymdegradstab.2020.109403.

[34] G. Guidotti, M. Soccio, E. Bondi, T. Posati, G. Sotgiu, R. Zamboni, A. Torreggiani, F. Corticelli, N. Lotti, A. Aluigi, Effects of the blending ratio on the design of keratin/poly(butylene succinate) nanofibers for drug delivery applications, Biomolecules 11 (2021) 1194, https://doi.org/10.3390/biom11081194.

[35] S. Wang, Q. Xing, Study on properties and biocompatibility of poly (butylene succinate) and sodium alginate biodegradable composites for biomedical applications, Mater. Res. Express 9 (2022) 085403, https://doi.org/10.1088/2053-1591/ac896f.

[36] Q. Zhao, S. Gao, Poly (Butylene Succinate)/silicon nitride nanocomposite with optimized physicochemical properties, biocompatibility, degradability, and osteogenesis for cranial bone repair, J. Funct. Biomater. 13 (2022) 231, https://doi.org/10.3390/jfb13040231.

[37] G.C. Miceli, F.S. Palumbo, F.P. Bonomo, M. Zingales, M. Licciardi, Polybutylene succinate processing and evaluation as a micro fibrous graft for tissue engineering applications, Polym. (Basel) 14 (2022) 4486, https://doi.org/10.3390/polym14214486.

[38] M. Chen, Z. Jiang, Z. Qiu, Synthesis, thermal, and mechanical properties of fully biobased poly(hexamethylene 2,5-furandicarboxylate-co-diglycolate) copolyesters, Polym. (Guildf) 267 (2023) 125678, https://doi.org/10.1016/j.polymer.2023.125678.

[39] Y. Dong, J. Wang, Y. Yang, Q. Wang, X. Zhang, H. Hu, J. Zhu, Bio-based poly (butylene diglycolate-co-furandicarboxylate) copolyesters with balanced mechanical, barrier and biodegradable properties: a prospective substitute for PBAT, Polym. Degrad. Stab. 202 (2022) 110010, https://doi.org/10.1016/j.polymdegradstab.2022.110010.

[40] G. Guidotti, M. Soccio, C. Argentati, F. Luzi, A. Aluigi, L. Torre, I. Armentano, C. Emiliani, F. Morena, S. Martino, N. Lotti, Novel nanostructured scaffolds of poly (butylene trans-1,4-cyclohexanedicarboxylate)-based copolymers with tailored hydrophilicity and stiffness: implication for tissue engineering modeling, Nanomaterials 13 (2023) 2330, https://doi.org/10.3390/nano13162330.

[41] Biological evaluation of medical devices tests for in vitro cytotoxicity, Definitive (2025).

[42] J. Devaux, P. Godard, J.P. Mercier, Bisphenol-A polycarbonate–poly(butylene terephthalate) transesterification. I. Theoretical study of the structure and of the degree of randomness in four-component copolycondensates, J. Polym. Sci. Polym. Phys. Ed. 20 (1982) 1875–1880, https://doi.org/10.1002/pol.1982.180201010.

[43] M. Manfroni, A. Coatti, M. Soccio, V. Siracusa, E. Boanini, E. Salatelli, N. Lotti, Eco-design of biobased poly(butylene succinate-b-pentamethylene 2,5-furanoate) copolymers with optimized mechanical, thermal and barrier properties for flexible food-packaging, Eur. Polym. J. 225 (2025) 113728, https://doi.org/10.1016/j.eurpolymj.2025.113728.

[44] M. Soccio, N. Lotti, M. Gigli, L. Finelli, M. Gazzano, A. Munari, Reactive blending of poly(butylene succinate) and poly(triethylene succinate): characterization of the copolymers obtained, Polym. Int. 61 (2012) 1163–1169, https://doi.org/10.1002/pi.4195.

[45] M. Gigli, N. Lotti, M. Gazzano, L. Finelli, A. Munari, Novel eco-friendly random copolyesters of poly(butylene succinate) containing ether-linkages, React. Funct. Polym. 72 (2012) 303–310, https://doi.org/10.1016/j.reactfunctpolym.2012.02.013.

[46] Y. Tian, H. Hu, C. Chen, F. Li, W. Bin Ying, L. Zheng, J. Wang, R. Zhang, J. Zhu, Enhanced seawater degradation through copolymerization with diglycolic acid: synthesis, microstructure, degradation mechanism and modification for antibacterial packaging, Chem. Eng. J. 447 (2022) 137535, https://doi.org/10.1016/j.cej.2022.137535.

[47] G. Wang, Y. Wu, Polylactic acid/poly(butylene diglycolate-co-butylene terephthalate) blends with improved toughness, Polym. Bull. 81 (2024) 10351–10367, https://doi.org/10.1007/s00289-024-05198-w.

[48] C. Gualandi, M. Soccio, E. Saino, M.L. Focarete, N. Lotti, A. Munari, L. Moroni, L. Visai, Easily synthesized novel biodegradable copolyesters with adjustable properties for biomedical applications, Soft Matter 8 (2012) 5466, https://doi.org/10.1039/c2sm25308a.

[49] M. Fabbri, M. Soccio, M. Gigli, G. Guidotti, R. Gamberini, M. Gazzano, V. Siracusa, B. Rimini, N. Lotti, A. Munari, Design of fully aliphatic multiblock poly(ester

urethane)s displaying thermoplastic elastomeric properties, Polym. (Guildf) 83 (2016) 154–161, https://doi.org/10.1016/j.polymer.2015.12.022.
[50] G. Guidotti, R. Duelen, N. Bloise, M. Soccio, M. Gazzano, A. Aluigi, L. Visai, M. Sampaolesi, N. Lotti, The ad hoc chemical design of random PBS-based copolymers influences the activation of cardiac differentiation while altering the HYPPO pathway target genes in hiPSCs, Biomater. Adv. 154 (2023) 213583, https://doi.org/10.1016/j.bioadv.2023.213583.
[51] H. Chen, M. Gigli, C. Gualandi, R. Truckenmüller, C. Van Blitterswijk, N. Lotti, A. Munari, M.L. Focarete, L. Moroni, Tailoring chemical and physical properties of fibrous scaffolds from block copolyesters containing ether and thio-ether linkages for skeletal differentiation of human mesenchymal stromal cells, Biomaterials 76 (2016) 261–272, https://doi.org/10.1016/j.biomaterials.2015.10.071.
[52] H. Hu, C. Lin, Q. Luan, X. Jiang, X. Zhang, Q. Wang, Y. Dong, J. Wei, J. Wang, J. Zhu, Synergistic modification of PBT with diglycolic acid and succinic acid: fast crystallization and high strength-toughness copolyesters for environmentally degradable packaging, ACS Sustain. Chem. Eng. 11 (2023) 14068–14080, https://doi.org/10.1021/acssuschemeng.3c03394.